Int J Fract (2006) 139:477–493
DOI 10.1007/s10704-006-0054-y

ORIGINAL ARTICLE

Numerical studies on crack problems in three-layered elastic media using an image method

Xi Zhang · Robert G. Jeffrey

Received: 29 November 2005/ Accepted: 27 February 2006

Abstract Two-dimensional crack problems in a three-layered material are analyzed numerically under the conditions of plane strain. An image method is adopted to obtain fundamental solutions for dislocation dipoles in trilayered media. The governing equations for equilibrium cracks can be constructed by distributed dislocation technique and their solutions are sought in terms of the displacement discontinuity method (DDM). Comparisons are made with available analytical or reference solutions for several examples at various contrasts of material constants, and good agreements are found. A crack within a brittle adhesive layer joining two semi-infinite blocks can propagate in a variety of ways. In particular, crack paths in the form of sigmoidal waves within the adhesive layer are revisited to reveal the sensitivities of cracking paths to initial crack locations and directions and residual stresses. In addition, Z-shape and H-shape cracks alternating from interface to interface are re-examined to highlight the transition of failure modes and the role of the interlayer thickness.

Keywords Layered media · Crack problem · Green's functions · Image method · DDM

X. Zhang (✉) · R. G. Jeffrey
CSIRO Petroleum Resources, Private Bag 10, Clayton South, VIC 3169, Australia
e-mail:xi.zhang@csiro.au

1 Introduction

Layered structure technologies are essential to composites, adhesive joints, microelectronic and optoelectronic devices (Hutchinson and Suo 1992), and are commonly encountered in geological settings (Pollard and Aydin 1988). For instance, a typical laminate structure for aeroplanes and space shuttles is an alternating stack of aluminum alloys sheets and fiber-reinforced epoxy. Layered ceramics of an alternating stack of TZ-3Y (3 mol% Y_2O_3-stabilized tetragonal ZrO_2) and Al_2O_3 provides a new and intriguing dimension for application since this material is very heat resistant (see an extended review by Chan (1997)). Furthermore, sedimentary rocks are, by their nature, layered (Price and Cosgrove 1990). However, defects such as cracks, flaws, inclusions and dislocations are inevitable in these layered materials and their propagation or multiplication always determine the stability or reliability of the layered structures. On one hand, the distribution of excessive defects concentrated over a small area can cause catastrophic failure of a material. On the other hand, one of the most interesting advancements in material science is to deliberately introduce weak interfaces in layered ceramics to promote crack deflection and directionally unstable crack growth, so as to increase material toughness. Understanding of failure mechanisms of these layered materials definitely is of current technological interest and much

attention has been paid to this topic during the past two decades.

The current study will focus on numerical simulation of possible crack propagation paths in a three-layered structure by alternating layers of two dissimilar, but isotropic elastic, brittle materials. This requires accurate treatment of discontinuities in elastic properties and residual stresses. There have been a number of investigations of the two-dimensional stress fields around a straight crack lying in the middle layer or along the interface (Hilton and Sih 1971; Fleck et al. 1991). However, it has been observed experimentally that in a sandwich specimen, the cracks can meander within the layer in a wavy form or in an alternating mode of switching back and forth between interfaces (Chai 1987; Akisanya and Fleck 1992). The natural weak bedding contacts between rock stratas provide an efficient resistance to dike emplacement (Delaney et al. 1986) due to stress contrasts in different layers and to the interface properties. Deflection of the cracks takes place at the interface it impinges on and a delamination crack then forms. The use of weak interfaces to facilitate crack deflection has been studied by Folsom et al. (1994) based on stress transition and vanishing interfacial toughness. Plane-strain delamination is examined by Akisanya and Fleck (1992) for a Z-shape crack alternating from interface to interface and by Lu (1996) and Suiker and Fleck (2004) for an H-shape crack connecting two interfaces. Importantly, advancing interface cracks can kink out of the interface into one of the adjoining materials (He et al. 1991). Most of these studies employed the finite element method (FEM) to investigate the sensitivity of crack paths to the modulus mismatch of layers and to the relative toughness of layer and interface.

For stress and strain analyses in layered materials, complicated integral transform methods such as Fourier Transform are usually employed to solve the crack problems (Peirce and Siebrits 2001). However, the crack is required to be parallel or perpendicular with regard to interfaces. Generally speaking, crack problems in layered structures can also be analyzed by either the domain-discretization methods (e.g., FEM) or the boundary element method (BEM). However, extremely fine finite-element meshes are required for accurate estimate of stress intensity factors that must be calculated to select crack paths. In this study, we employ the image method proposed by Aderogba (2003) to derive the Green's functions for a singularity in the trimaterial from the known exact solutions for bimaterial cases. By means of Green's functions, a BEM-based discretization method, the DDM, is then used to obtain stress intensity factors and stress and deformation fields for the crack problem. This methodology retains the advantages of BEM since the discretization is only required along the cracks.

In this paper, the initiation phase of a crack is not considered and the crack is assumed to grow from a small pre-existing crack in the mid-layer. A numerical model is proposed to assess the stress intensity factors for a variety of crack geometries. The crack growth is assumed to be driven by an internal pressure associated with injected fluid as would occur for hydraulic fractures, which are widely used in the oil and gas industry. The stress intensity factors and the crack opening profiles are examined, as well as the selection of the crack paths. In addition, the complex interfacial stress intensity factors for Z-shape and H-shape cracks on interfaces are also re-examined in details. Prior to presenting numerical results, comparisons with existing solutions of stress intensity factors and crack surface profiles for various crack configurations are made to confirm the accuracy of numerical results.

2 Green's functions

Consider a crack problem associated with a three-layer elastic medium as shown in Fig. 1. The x_1-axis is taken to be the upper interface and the Cartesian coordinate system used is depicted in Fig. 1. Suppose that the middle elastic layer with thickness $H(|x_1| < \infty, -H < x_2 < 0$ and moduli $(\mu_2, \nu_2))$ is perfectly bonded to two semi-infinite solids $|x_1| < \infty, 0 < x_2 < \infty$ and $|x_1| < \infty, -\infty < x_2 < -H$ of moduli (μ_1, ν_1) and (μ_3, ν_3), respectively. The governing equations for the plane problems in an isotropic elastic solid are summarized as follows. In the absence of any body force, the field equations of equilibrium, elasticity and geometric relations valid for each layer are:

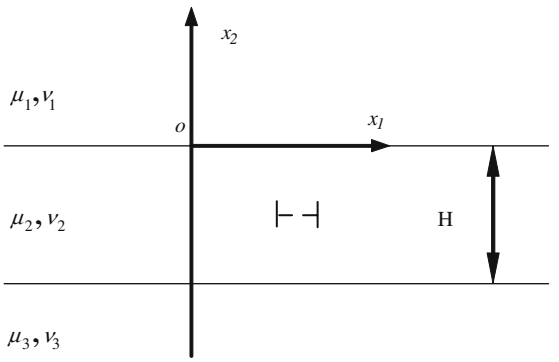

Fig. 1 A dislocation dipole located within the interlayer

$$\sigma_{ij,j} = 0 \tag{1}$$

$$\sigma_{ij} = 2\mu \left[\varepsilon_{ij} + \frac{\nu}{1-2\nu} \varepsilon_{kk} \delta_{ij} \right] \tag{2}$$

$$\varepsilon_{ij} = \tfrac{1}{2} \left(u_{i,j} + u_{j,i} \right) \tag{3}$$

where σ_{ij} is the Cauchy stress tensor, ε_{ij} is the strain tensor, and u_i is the displacement vector, μ is the shear modulus, ν is the Poisson's ratio, and δ_{ij} is the Kronecker's delta.

In the two-dimensional cases, the solutions can be obtained by means of the Airy stress function ϕ, which is a biharmonic function. In particular, displacements and stresses for each layer can be expressed as follows:

$$2\mu u_i = -\phi_{,i} + (1-\nu) \int \nabla^2 \phi \, \mathrm{d}x_i \tag{4}$$

$$\sigma_{ij} = \delta_{ij} \phi_{,kk} - \phi_{,ij} \tag{5}$$

where ∇^2 is the two-dimensional Laplacian operator. It should be mentioned that the index for material number is dropped in the above equations.

For the analysis of crack problems in the three-layered materials, if the Airy stress functions for a singularity like a dislocation dipole are known for each material, the fundamental stress and displacement fields can be obtained by Eqs. (4) and (5). Furthermore, a crack can be simulated by an array of distributed dislocation dipoles. In preparation for deriving the Green's functions for a dislocation dipole, we first recall its solutions in an infinite homogeneous elastic medium. The detailed formulae for eigenstress solutions in homogeneous materials can be found in Appendix A, which were obtained by utilizing Eshelby's theorem and Kelvin solutions.

The image method can be applied to two-dimensional elastostatics in the case of bimaterials separated by a flat interface. Consider the upper layer ($x_2 > 0$) is occupied by an elastic medium with corresponding moduli (μ_1, ν_1) and the lower layer ($x_2 < 0$) is filled by a different elastic medium with corresponding moduli (μ_2, ν_2). It is supposed that an arbitrary singularity is located in the upper layer. According to the work by Aderogba (1977) to satisfy continuity and equilibrium conditions across the interface, the new Airy stress functions for the upper and the lower planes, respectively, are given by

$$\Psi_1 = L_1 \Phi_0(x_1, x_2, -p_1, p_2) \tag{6}$$

$$\Psi_2 = L_2 \Phi_0(x_1, x_2, p_1, p_2) \tag{7}$$

where the operators L_1 and L_2 are given in Appendix B, Φ_0 is the Airy stress function for a singularity in an infinite elastic medium and the dislocation dipole is located at (p_1, p_2) and the influenced point is at (x_1, x_2). Based on the Airy stress functions obtained, we can carry out the calculations for stress components based on Eq. (5). It should be mentioned that there is a sign difference in the operator L_1 between the edge and the glide dislocation dipoles. In addition, the choice of Airy stress functions for each layer depends on whether the dislocation dipole is located within it or not. By rearranging the material constants for upper and lower layers, we can find solutions for the cases when dislocation dipoles are located in the lower half plane. The Green's functions for the singularity in a trimaterial can be obtained through an image method or an alternating technique described by Aderogba (2003). At first, disregarding the $x_2 = -H$ interface, the regions 2 and 3 are treated as a homogeneous medium of material 2. The Airy stress functions for each region can be constructed based on Eqs. (6) and (7). However, the solutions cannot ensure stress and displacement continuity at the interface $x_2 = -H$ or in the third material. Secondly, disregarding the existence of the $x_2 = 0$ interface, the regions 1 and 2 are considered as a homogeneous medium of material 2. We must take into account the stresses and displacements induced by both the source singularity and its image with respect to $x_2 = 0$. Accordingly,

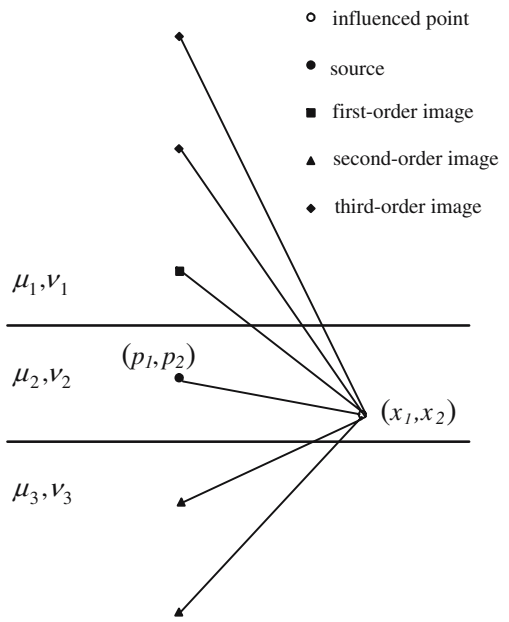

Fig. 2 Schematics of the image method

the Airy stress functions for each discontinuity can be obtained through satisfying the continuity conditions at the $x_2 = -H$ interface. Next, repeat the above process by invoking Eqs. (6) and (7) at the interface $x_2 = 0$ for the two images with respect to $x_2 = -H$. The process is continued indefinitely for this trilayered material, leading to an infinite series of images. A schematic description of this process for the case with both singularity source and influenced point located in the middle layer is depicted in Fig. 2. More detailed description has been provided in Appendix C. In particular, if the dislocation dipole (p_1, p_2) and the influenced point (x_1, x_2) are located in the layer and the dipole produces a unit vertical opening, the corresponding Airy stress functions for the source and its images Φ_i are given by

1. the singularity source

$$\Phi_0 = -\frac{t^2}{s^2+t^2} - \frac{1}{2}\log(s^2+t^2) \tag{8}$$

where $t = x_1 - p_1$ and $s = x_2 - p_2$.

2. the first-order image

$$\Phi_1 = \frac{At^2}{\bar{s}^2+t^2} - \frac{2A(\bar{s}^2-t^2)(\bar{s}-v)v}{(\bar{s}^2+t^2)^2} + \frac{1}{4}(A+B)\log(\bar{s}^2+t^2) \tag{9}$$

where $\bar{s} = x_2 + p_2$ and $v = x_2$ and A and B are material constants defined by Eq. (B.3) in Appendix B.

3. the second-order image

$$\Phi_2 = \frac{\hat{s}[BC(\hat{s}-u)+ADv]}{\hat{s}^2+t^2} - \frac{AH[-3\hat{s}^3+\hat{s}^2t+2H(\hat{s}^2-t^2)]}{(\hat{s}^2+t^2)^2} + \frac{8AC(\hat{s}^2-3t^2)(\hat{s}-u)Hv}{(\hat{s}^2+t^2)^2} - \frac{1}{4}\log(\hat{s}^2+t^2) \tag{10}$$

where $\hat{s} = x_2 - p_2 + 2H$ and C and D are the derived material constants associated with the $x_2 = -H$ interface in terms of the same definitions as A and B, respectively.

In the calculation presented below, the Airy stress functions of up to the eighth-order image have been employed. It is found that the sum of the first eight terms can provide a good approximation for most combinations of materials, as verified in the next section.

3 Problem formulation and numerical method

The formulation and solution of crack problems is simplified by application of distributed dislocation dipole singularities (Hills et al. 1996). The crack is modeled by a continuous distribution of dislocation dipoles and solutions are sought for the resulting integral equations based on the equations of equilibrium. In the absence of shear stress along the crack and body force, the integral equations are:

$$\sigma_n(\mathbf{x}) - \sigma_1(\mathbf{x}) = \sum_{m=1}^{M}\int_0^{l_m}[G_{nn}(\mathbf{x},\ell,\alpha,\beta)\omega(\ell) + G_{ns}(\mathbf{x},\ell,\alpha,\beta)\upsilon(\ell)]\,\mathrm{d}\ell \tag{11}$$

$$-\tau_1(\mathbf{x}) = \sum_{m=1}^{M}\int_0^{l_m}[G_{sn}(\mathbf{x},\ell,\alpha,\beta)\omega(\ell) + G_{ss}(\mathbf{x},\ell,\alpha,\beta)\upsilon(\ell)]\,\mathrm{d}\ell \tag{12}$$

where $\mathbf{x} = \{x_1, x_2\}$, ℓ is the arc length of the crack and M is the number of elements. $\omega(s)$ and $\upsilon(s)$ are the crack opening and shear displacement discontinuities across the fracture, respectively. l_m is the length for each crack with a subscript index

associated with the crack number. σ_n is the normal traction on the crack surface and σ_1, τ_1 are normal and shear stresses on the crack surface induced by far-field and residual stresses. G_{nn}, G_{ns}, G_{sn} and G_{ss} are the hypersingular Green's functions derived by differentiating the Airy stress functions for the dislocation dipole problems in light of Eq. (5). α and β are two Dundurs' parameters defined in Appendix B. For the sake of facilitating comparisons with existing results, both the upper and the lower planes are assumed to be the same material in the following.

For inclined cracks, there is a coordinate transformation to relate the normal and tangential stresses to the normal and tangential displacement discontinuities along the crack surface within the framework of a local coordinate system. See Appendix D for more general expression of the equations of equilibrium. The numerical analyses are carried out using the DDM with a constant strength for each element. The tip element has an imposed shape function as given by the LEFM solution at the tip. The hypersingular integrals are evaluated analytically, while the regular integrals are evaluated numerically for each element. Based on the nodal displacements, Eqs. (11) and (12) can be represented by a set of matrix relations. In particular, after eliminating shear displacements, the final matrix form can be rearranged as follows

$$\mathbf{A}\{\omega\} = \mathbf{b} \tag{13}$$

where $\mathbf{A}$ is a matrix assembled from the Green's functions, and $\mathbf{b}$ and $\{\omega\}$ are the vectors for the traction and the crack opening, respectively.

In terms of the displacement discontinuities obtained, the mode I and II stress intensity factors for the tip within the interlayer are obtained by the displacement correlation method

$$(K_{\mathrm{I}}, K_{\mathrm{II}}) = \lim_{r\to 0} \frac{\mu_2}{\kappa_2 + 1}\sqrt{\frac{2\pi}{r}}[\omega(r), \upsilon(r)] \tag{14}$$

where $\kappa_2 = 3 - 4\nu_2$. If the crack tip is on the interface, the complex stress intensity factor is given as follows (Hutchinson et al. 1987)

$$K_1 + iK_2 = \lim_{r\to 0} \frac{(1+2i\epsilon)}{2[(1-\nu_1)/\mu_1 + (1-\nu_2)/\mu_2]} \times\sqrt{\frac{2\pi}{r}}[\omega(r) + i\upsilon(r)]r^{-i\epsilon} \tag{15}$$

where $\epsilon = \ln[(1-\beta)/(1+\beta)]/2\pi$.

3.1 Validation

To validate the Green's functions, examples are presented in this subsection, by comparing our results with those given by Fett and Munz (1997) for interlayer cracks and the analytical solution for interfacial cracks given by Hutchinson et al. (1987). Figures 3 and 4 shows the variations of the normalized toughness for different modulus contrasts and geometry configurations of horizontal and vertical cracks located within the interlayer. The toughness is normalized by $\sigma\sqrt{2\pi a}$ in which σ is the uniform internal pressure along the crack and a is the half crack length. The scattered symbols are based on the results given in the monograph by Fett and Munz (1997). The numerical results obtained here, shown by solid lines, match very well with their counterparts. The relative small discrepancies within 10% of the results collected by Fett and Munz (1997) may result from discretization used in both numerical models. Only 50 elements are used in the calculation, and the numerical results for increasing number of elements are convergent to the results provided here.

For an interface crack subjected to uniform internal pressure σ, the relative crack surface displacements are given by Hutchinson et al. (1987) as follows,

$$\omega + i\upsilon = \frac{\sigma\sqrt{a^2 - x^2}}{C\sqrt{1-\beta^2}}\left|\frac{x+a}{x-a}\right|^{i\varepsilon} \tag{16}$$

where x denotes the distance to the center of the crack, and

$$C = \frac{2\mu_1(1+\alpha)}{(\kappa_1+1)(1-\beta^2)} = \frac{2\mu_2(1-\alpha)}{(\kappa_2+1)(1-\beta_2)} \tag{17}$$

and the corresponding complex interface stress intensity factor for the right tip is

$$K_1 + iK_2 = \sigma\sqrt{\pi a}(2a)^{-i\epsilon}(1+2i\epsilon) \tag{18}$$

Figure 5 provides the normalized crack opening and sliding displacements for the interface crack. The interface crack is treated as the crack on the upper interface for a three-layered structure and its length $2a$ is extremely small compared with the interlayer thickness. It is found that the numerical results based on 100 elements match the analytic solutions very well in Fig. 5. The corresponding

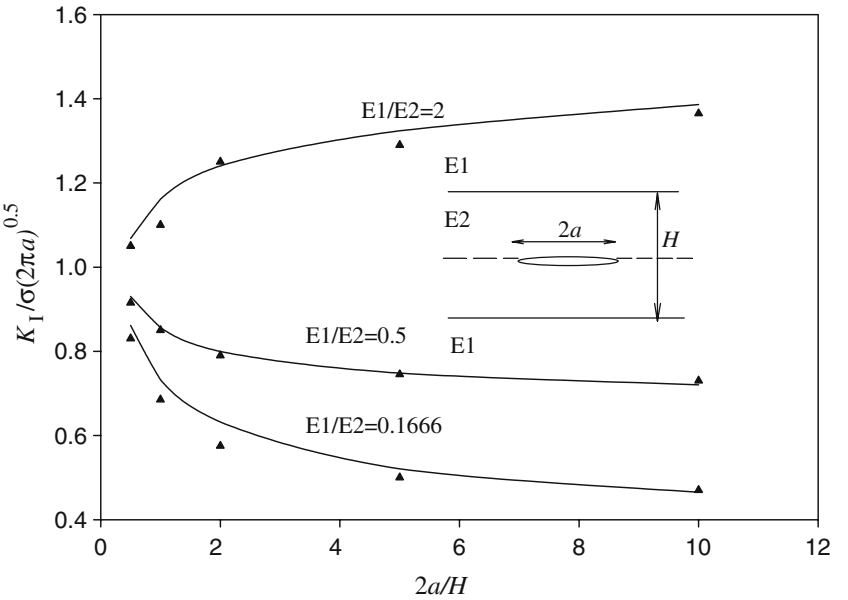

Fig. 3 Comparisons of normalized toughness for the cracks parallel to the interfaces with the results (the scattered symbols) collected by Fett and Munz (1997)

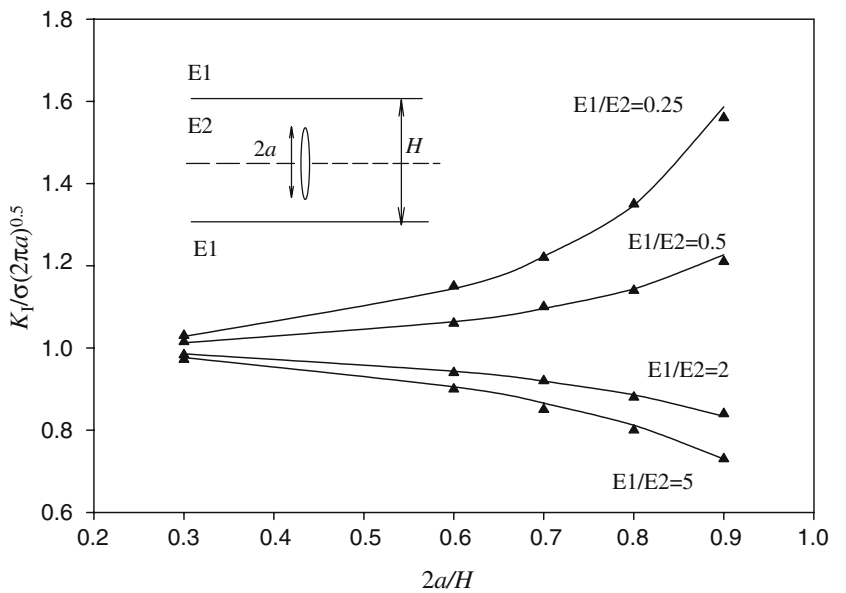

Fig. 4 Comparisons of normalized toughness for the cracks vertical to the interfaces with the results (the scattered symbols) collected by Fett and Munz (1997)

analytic complex interface stress intensity factor can therefore be recovered.

4 Numerical results

4.1 Sigmoidal crack paths

To begin with, the propagation path of a uniformly pressurized slant crack in an inhomogeneous material can be modeled by the proposed numerical method. We choose the uniform pressure loading case because we are motivated by layered problems involving hydraulic fracturing. The interlayer with thickness H is perfectly bonded by two stiffer half planes. The elastic properties E and ν are specified for the interlayer and the internal pressure p is adjusted to meet the material toughness K_{IC}. A residual tensile stress σ_{res} exists in the layer, which is represented by a normal remote load parallel to the interfaces. The selection of crack propagation

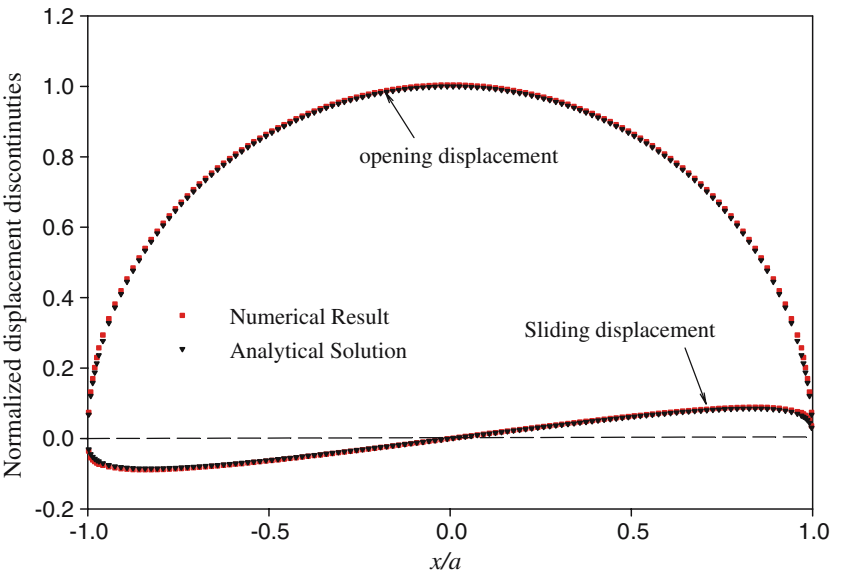

Fig. 5 Comparisons of normalized crack flank displacements for an interface crack subjected to uniform internal pressure with the analytic solutions given by Hutchinson et al. (1987)

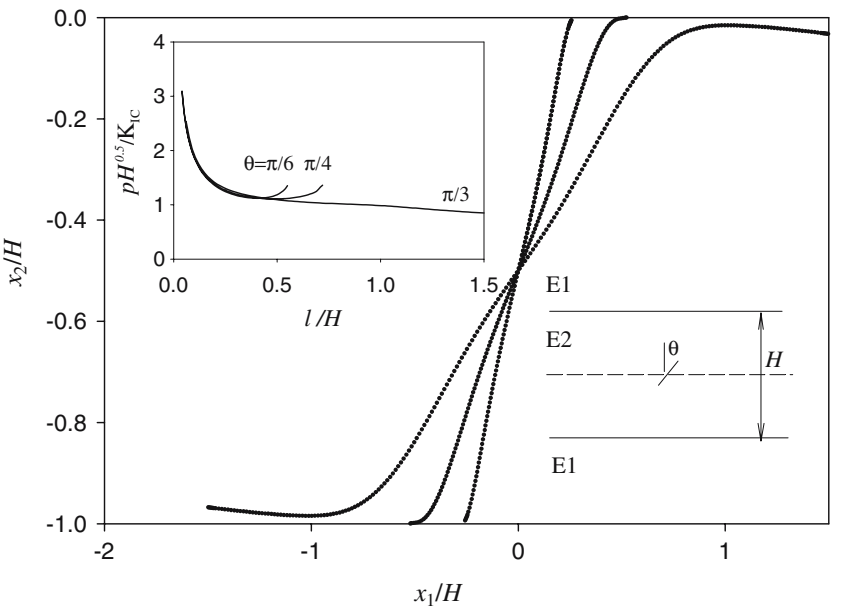

Fig. 6 Trajectories and variations of internal pressure of uniformly pressurized cracks starting from the middle plane of the interlayer for various inclined angles ($\chi = 0.01$)

direction is assumed to follow the maximum tensile stress criterion proposed by Erdogan and Sih (1963). Dimensional analysis dictates that

$$\frac{p\sqrt{H}}{K_{\mathrm{IC}}} = \tilde{p}(\bar{\ell}, \chi, \theta, \alpha, \beta) \tag{19}$$

$$\left\{\frac{x_1}{H}, \frac{x_2}{H}\right\} = \{f_1, f_2\}(\chi, \theta, \alpha, \beta) \tag{20}$$

where $\bar{\ell} = \ell/H$ with ℓ being the half arc length of the growing crack and $\chi = \sigma_{\mathrm{res}}\sqrt{H}/K_{\mathrm{IC}}, \theta$ is the inclined angle of the initial crack with respect to the interfaces. The initial crack length is assumed to be too small to perturb the stress fields on the interface, with its center on the middle plane of the interlayer.

Figure 6 shows the propagation paths and the variations of normalized internal pressure

$p\sqrt{H}/K_{\mathrm{IC}}$ for three different crack angles at $\chi = 0.01$. They are plotted as against the inclined angles $\theta = \pi/6, \pi/4$ and $\pi/3$ in Fig. 6. The interlayer occupied the domain $-1 < x_2/H < 0$ and material constants are $E_2/E_1 = 6$ and $\nu_1 = \nu_2 = 0.3$, corresponding to a pair of Dundurs parameters $(\alpha_{21}, \beta_{21}) = (0.714, 0.204)$ with α_{21}, β_{21} as the Dundurs parameters for the elastic mismatch from material 2 to material 1. It is seen that the crack paths exhibit a sigmoidal shape. When θ is less than $\pi/4$, the crack tends to intersect the interfaces. However, if θ is larger than $\pi/4$, the crack avoids the interface by turning back from the interfaces. It is interesting to note that such sigmoidal crack paths have been experimentally found in layered ceramics (see Chan 1997). It is noted from Fig. 6 that the internal pressure is insensitive to the crack pathways if the crack tip is not very close to the interface. When the crack is within the vicinity of the interface, for example, there is an increase in internal pressure, if θ is less than $\pi/4$.

4.2 Wavy crack paths

A wavy crack trajectory about the midplane of the interlayer is anticipated when $\partial K_{\mathrm{II}}/\partial a > 0$ and with a positive T-stress (Fleck et al. 1991). Therefore, a pre-existing crack located slightly above or below the midplane can give rise to wavy crack paths under tensile residual stresses. Although Fleck et al. (1991) has pointed out the existence of wavy crack paths, there is no crack path simulation available in literature, to our knowledge. Figure 7 shows the crack trajectories and the variations of normalized internal pressure $p\sqrt{H}/K_{\mathrm{IC}}$ for a small pre-existing crack parallel to the interfaces, and with an offset to the middle line. The material constants are the same as those used in the previous subsections. Except for the dimensionless parameter χ, the crack trajectories depend on the length ratio $\varpi = s/H$ in which s is the distance of the pre-existing crack to the middle line. $\varpi = -0.25$ is employed for the two values of χ. There is a uniform internal pressure along the crack, which is adjusted based on the toughness and the propagation direction is also based on the maximum tensile stresses criterion given by Erdogan and Sih (1963). It is demonstrated in Fig. 7 that the crack propagates in a wavy form and the wave length seems to increase with decreasing the value of χ. In addition, there is a slight difference in variations of internal pressure between $\chi = 0.3$ and 0.4 if the tip is not close to the upper interface. The halt in the decreasing trend of internal pressure can be detected for $\chi = 0.4$ when the crack tip is close to the upper interface. But when the crack tip leaves the interface at a certain distance, the internal pressure resumes its decreasing trend.

4.3 Z-shape cracks

A crack in a brittle adhesive layer can grow in an alternating way between two interfaces. To simplify the crack problems, let us consider the Z-shape crack geometry as shown in Fig. 8. The left branch on the lower interface is a semi-infinite cut and the right branch on the upper interface is an interface crack. Both branches are connected by a vertical cut subjected to an internal pressure σ_{o}. This alternating morphology has been documented for mode I loading of an aluminum/epoxy/aluminum sandwich specimen by Chai (1987). Material constants of two elastic media are selected so that $\beta_{21} = \alpha_{21}/4$ and $\nu_1 = \nu_2 = 1/3$. The crack is loaded by the tensile residual stress within the interlayer only. The induced complex interface stress intensity factor for the crack branch on the upper interface is shown in Fig. 8. As done by Suo and Hutchinson (1989), the interlayer thickness is chosen as the reference length to normalize the complete interface stress intensity factor. Therefore, Eq. (15) can be rewritten as

$$KH^{i\epsilon} = \lim_{r\to 0} \frac{(1+2i\epsilon)}{2[(1-\nu_1)/\mu_1 + (1-\nu_2)/\mu_2]} \times\sqrt{\frac{2\pi}{r}}[\omega(r) + i\upsilon(r)]\left(\frac{H}{r}\right)^{i\epsilon} \tag{21}$$

where $K = K_1 + iK_2$ and the phase angle of the interfacial crack is defined as

$$\Psi = \arctan\left[\frac{\mathrm{Im}(Kh^{i\epsilon})}{\mathrm{Re}(Kh^{i\epsilon})}\right] \tag{22}$$

A plot of the normalized real and imaginary parts of the complex interface stress intensity factors (by $\sigma_{\mathrm{o}}\sqrt{H}$) versus the normalized crack length l/H is shown in Fig. 8. Under given crack geometry and loading configuration, the opening along the

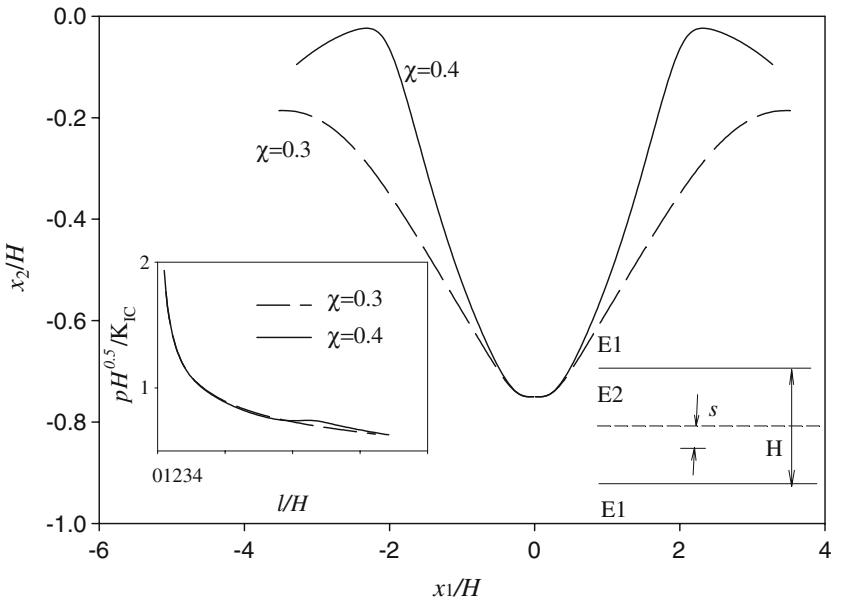

Fig. 7 Trajectories and variations of internal pressure of uniformly pressurized cracks initially parallel to the interfaces and with an offset to the midplane ($\varpi = -0.25$)

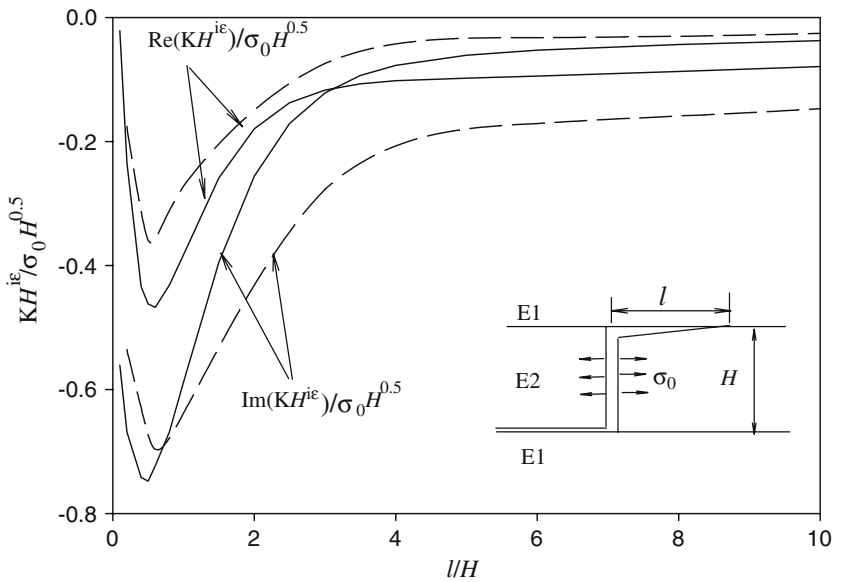

Fig. 8 Dimensionless complex interface stress intensity factors versus the length ratio l/H for Z-shape cracks under tensile residual stress. The solid lines are based on the proposed model and the dashed lines are finite element results obtained by Akisanya and Fleck (1992)

crack is predicted to be negative. The solid lines are based on the results obtained here and the dashed lines are from Akisanya and Fleck (1992). The real and imaginary parts both have a minimum value at $l/H \sim 0.55$. With increasing the length ratio l/H beyond 0.55, the imaginary part increases faster than the real one. Finally both components tend to approach zero. However, the magnitude of real part is larger than that of imaginary one at large length ratio l/H based on our numerical results, while the magnitude of real part is still larger than the imaginary one in Akisanya and Fleck (1992). The varying trend of $KH^{i\epsilon}$ based on relatively small K_2 with respect to K_1 reflects the transition of failure modes to a tensile interfacial crack ultimately for a Z-shape crack, as argued by Suo and Hutchinson (1992).

In addition, the failure mode transition can be represented by the interfacial phase angle Ψ. Its variation is plotted against the length ratio l/H in Fig. 9. As expected, the interface cracks start with a shear-dominated crack growth correspond-

ing to $\Psi \sim 90$ degree. The large negative imaginary components at the early stage will force the crack to grow along the interface. As the crack advances, the curve tends to resemble the solution of the interfacial crack on the upper interface with a small shearing component (Hutchinson and Suo, 1992). This transition from shearing to tensile failure mode can be easily detected in Fig. 9 and it is anticipated that the phase angle will approach the dashed-dot-dot line which indicates the solution obtained by Suo and Hutchinson (1989) for a long interfacial crack on the upper interface. The phase angle of infinite interface cracks is -10.5 degree for the given material constants by Suo and Hutchinson (1989). However, the phase angle curve in the dashed line based on the numerical results obtained by Akisanya and Fleck (1992) shows a different trend.

Furthermore, the variation of the interfacial phase angle of the right tip with the crack length for an interfacial crack on the upper interface is calculated numerically, as depicted in Fig. 10 based on the material constants specified above. When $a/H = 0.5, \Psi = 6.83$ degree at $\alpha = 0.8$ and $\beta = \alpha/4$, which is close to the bimaterial solution $\Psi = 7.35$ degree from the theoretical solutions given by Hutchinson et al. (1987). Figure 10 also shows that there is a small discrepancy in the phase angle for a/H up to 40, between our numerical model and the asymptotic solution ($\Psi = -10.5$ degree) obtained by Suo and Hutchinson (1989).

4.4 H-shape cracks

In fiber-reinforced ceramic composites, loading in the direction of the fibers gives rise to cracks in the fiber bundles. Then the fibre-bundle cracks propagate into a matrix-rich region parallel to the loading direction, and then bifurcate to form H-shape cracks. Plane-strain analysis of H-shape cracks has been conducted by Lu (1996), in which for simplicity, the fibers and the matrix have the same material constants. Figure 11 shows the interfacial phase angles as a function of $2a/H$ for different combinations of material constants. It should be mentioned that the case of $\alpha_{21} = \beta_{21} = 0$ corresponds to the assumption of material homogeneity by Lu (1996). The circles in Fig. 11 are extracted from Fig. 6 in Lu (1996). It is seen that for $0.1 < 2a/H < 0.25$, our numerical results match very well the results of Lu (1996). For $2a/H < 0.1$, a discrepancy between two solutions is detected and seems to increase as $2a/H$ decreases. This may arise from different discretization schemes in the two numerical models. For small crack lengths, relatively large number of elements should be employed for the segment connecting two interfacial cracks to meet the requirement on accuracy.

There exists a transition in failure mode from mixed to shearing mode as displayed in Fig. 11. However, this transition takes place at small length ratios and finishes before $2a/H$ attains 0.3. This means that the H-shape crack is embedded with a large component of mode II stress intensity factor as $2a/H$ increases beyond 0.3.

5 Conclusions

In this paper, we have first presented an image method to derive the Green's functions for three-layered elastic media based on the formulation of the Airy stress functions proposed by Aderogba (2003). The method can be applied to obtain the fundamental solutions for dislocation dipoles. Although the problem involves infinite series of images, the first eight terms are employed in the model and reasonable numerical accuracy is obtained in comparisons with existing results. The corresponding numerical method for equilibrium cracks is delineated following the procedure of the DDM. Numerical examples are examined in the context of the existing studies for interfacial cracks or cracks within the interlayer. The comparisons between them show good agreements based on the eight-term Green's functions. In addition, based on the crack growth criterion, the sigmoidal and wavy paths of meandering cracks within the interlayer are recovered, consistent with experimental observations and theoretical predictions. On the other hand, the complex stress intensity factors for Z-shape and H-shape cracks on the interfaces alternating from one interface to another are obtained under tensile residual stresses or loads. The variations of their phase angles evidently imply the transition of failure modes from shear-dominated to opening-dominated crack

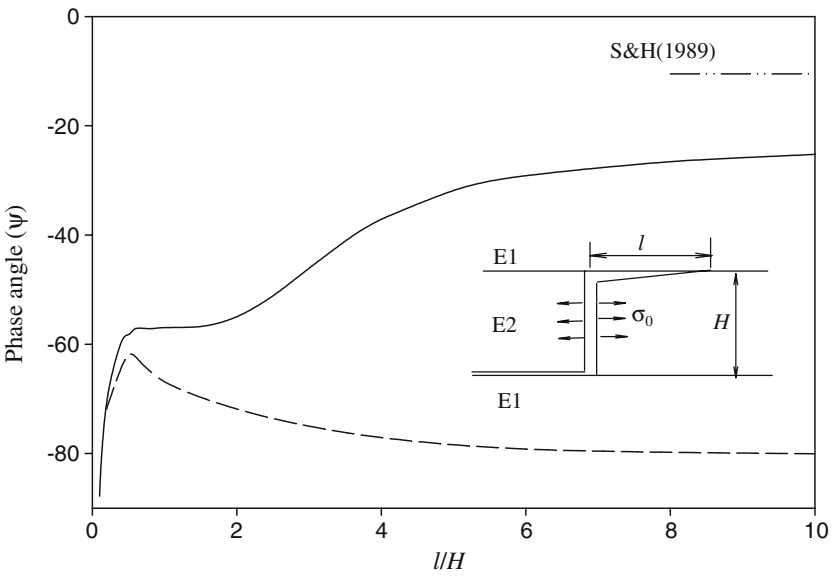

Fig. 9 Comparisons of interfacial phase angle for the Z-shape cracks subjected to tensile residual stress between numerical results (the solid line) and finite element solutions by Akisanya and Fleck (1992) (the dashed line). The phase angle for the limiting case ($l/H \to \infty$) (the dash-dot-dot line) is obtained by Suo and Hutchinson (1989)

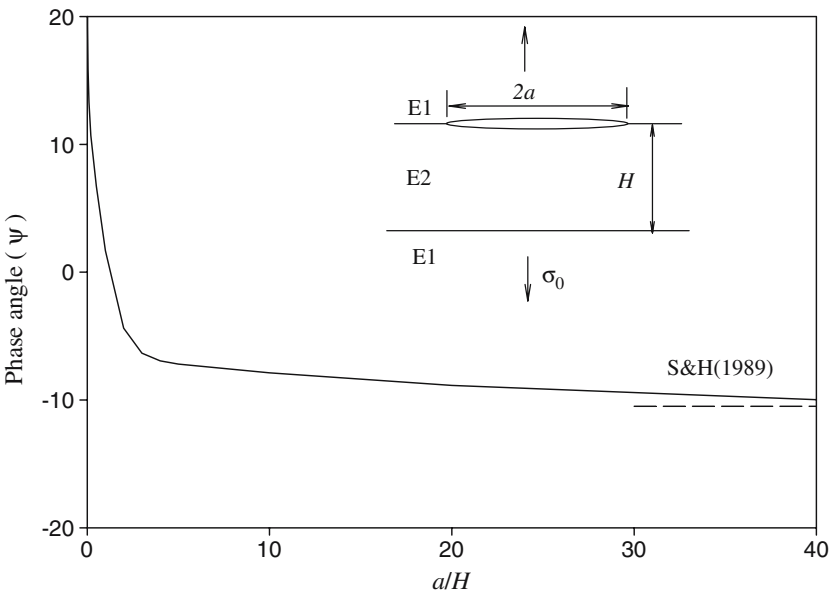

Fig. 10 Interfacial phase angle for the right tip of an interfacial crack on the upper interface. The phased angle obtained by Suo and Hutchinson (1989) for the limiting case ($a/H \to \infty$) is included by a dashed line

growth for Z-shape cracks. It is observed that the thickness of interlayers starts to play a role in the transition when the crack length is about the interlayer thickness. However, the transition of failure modes from mixed to shearing mode takes place at small crack lengths for H-shape cracks and subsequently H-shape cracks exhibit themselves as a shearing-dominant crack.

Appendix A: Eigenstress in infinite medium

In order to demonstrate clearly the establishment of the fundamental solutions for stresses and displacements in a full plane, we first recall briefly some basic solutions for a concentrated force in an infinite elastic medium and the Eshelby theorem for completeness.

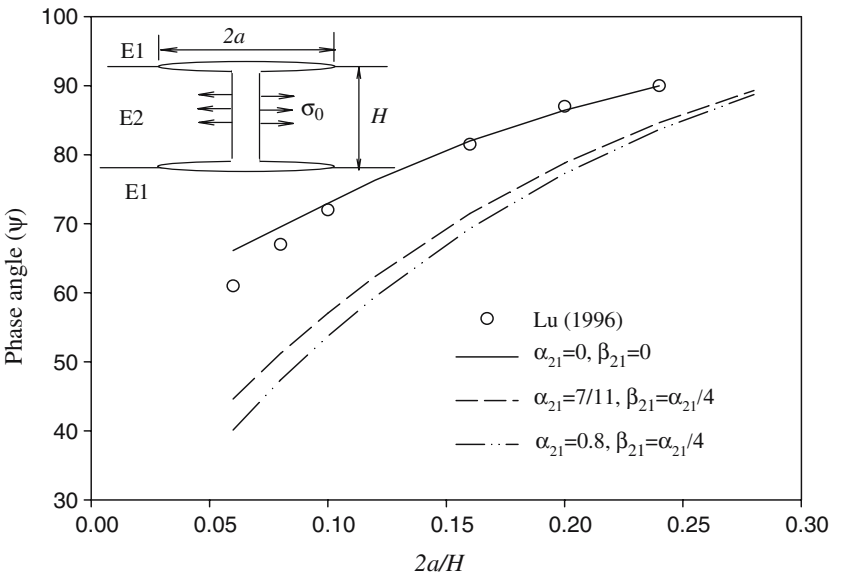

Fig. 11 Interfacial phase angle for the H-shape cracks subjected to tensile residual stress. The circles are extracted from the numerical results given by Lu (1996) for H-shape cracks in homogeneous materials

A.1 Kelvin's solution for a two-dimensional solid

Consider the Kelvin's problem, that is, a unit line force acting along x_j-axis, lying at point $\mathbf{x}' = (\mathbf{x}'_1, \mathbf{x}'_2)$ in an infinite elastic solid. The Airy stress functions for two-dimensional problems for unit line forces in x_1 and x_2 are given by

$$\phi^1 = \frac{1}{2\pi(\kappa+1)}[(\kappa-1)\xi \log r + (\kappa+1)\eta\theta] \quad \text{(A.1)}$$

$$\phi^2 = \frac{1}{2\pi(\kappa+1)}[(\kappa-1)\eta \log r + (\kappa+1)\xi\theta] \quad \text{(A.2)}$$

where $r = \sqrt{\xi^2+\eta^2}, \theta = \arctan[\eta/\xi]$, in which $\xi = x_1 - x'_1$ and $\eta = x_2 - x'_2$.

A.2 Dislocation dipoles and strain nuclei

Consider a slip plane S within an isotropic elastic material. The upper surface S^+ moves by the Burgers vector $\mathbf{b}$ relative to the lower plane S^-. Then the eigenstrains can be written as

$$e^T_{ij}(\mathbf{x}) = -\frac{1}{2}(b_i n_j + b_j n_i)\delta(\mathbf{S}-\mathbf{x}) \quad \text{(A.3)}$$

where $\delta(\mathbf{S}-\mathbf{x})$ is the Dirac delta satisfying

$$\int_\Omega \delta(\mathbf{S}-\mathbf{x})\,\mathrm{d}\mathbf{x} = \int_S \mathrm{d}s \quad \text{(A.4)}$$

As an example, the displacement u_2 experiences a finite constant jump at point $\mathbf{x}'$ along the $\mathbf{x}_1$ direction in a surface parallel to the plane $(x_1, 0)$. Hence, we have

$$u_2(x_1, x'_2+) - u_2(x_1, x'_2-) = b_2\delta(x_1)H(x_2) \quad \text{(A.5)}$$

where $H(x)$ is the Heaviside step function,

$$H(x) = \begin{cases} = 0 & x < 0 \\ = 1 & x > 0 \end{cases} \quad \text{(A.6)}$$

This problem can then modeled by distributed eigenstrain $e^T_{ij} = 0$ except for $e^T_{22} = b_2$ over the an infinitesimal surface with a center at $\mathbf{x}'$.

A.3 Eshelby theorem

In an elastic space, when a uniform eigenstrain e^T_{ij} is prescribed within an arbitrary closed subregion V, eigenstress σ^T_{ij} can be expressed in terms of e^T_{ij} by means of Hooke's law

$$\sigma^T_{ij} = 2\mu\left[e^T_{ij} + \frac{\nu}{1-2\nu}e^T_{kk}\delta_{ij}\right] \quad \text{(A.7)}$$

For some general cases, the displacement fields due to the disturbed eigenstresses can be expressed in a form:

$$u_i(\mathbf{x}) = \int_V u^j_i(\mathbf{x}, \mathbf{x}')f_j\,\mathrm{d}\mathbf{x}' \quad \text{(A.8)}$$

where $u^j_i(\mathbf{x}, \mathbf{x}')$ is the Green's function for the concentrated force which gives the value of the displacement components u_i at point $\mathbf{x}$ due to a point force in the direction j applied at point $\mathbf{x}'$, f_j is the

eigenforces. Actually, the eigenforces for a force doublet are given by

$$f_j = \sigma^T_{jk}(\mathbf{x}')\frac{\partial}{\partial x'_k} \tag{A.9}$$

see details in Mura (1987).

If we know the solutions ϕ^j for all Kelvin problems, the corresponding Airy stress function ψ for different dislocation dipoles can be obtained in terms of the Eshelby Theorem. In particular, it leads to

$$\psi = \sigma^T_{jk}\frac{\partial \phi^j}{\partial x'_k} \tag{A.10}$$

A.3.1 Edge dislocation dipoles

The eigenstresses caused by the unit eigenstrain $e^T_{11} = 1$ can be obtained as:

$$\sigma^T_{11} = (1-\nu)P, \quad \sigma^T_{12} = 0, \quad \sigma^T_{22} = \nu P \tag{A.11}$$

where $P = 2\mu/(1-2\nu)$. Then,

$$\psi^{11\infty} = \sigma^T_{kl}(\mathbf{x}')\frac{\partial}{\partial x'_l}\phi^j = \sigma^T_{11}\frac{\partial \phi^1}{\partial x'_1} + \sigma^T_{22}\frac{\partial \phi^2}{\partial x'_2} \tag{A.12}$$

Substituting ϕ^1 and ϕ^2 in the above equation, we have

$$\psi^{11\infty} = -\frac{2\mu}{\pi(\kappa+1)}\left(\log r - \frac{\cos 2\theta}{2}\right) \tag{A.13}$$

where $\cos 2\theta = [\xi^2 - \eta^2]/r^2$.

In the same way, the Airy stress function for the unit eigenstrain $e^T_{22} = 1$, is given by

$$\psi^{22\infty} = -\frac{2\mu}{\pi(\kappa+1)}\left(\log r + \frac{\cos 2\theta}{2}\right) \tag{A.14}$$

A.3.2 Glide dislocation dipoles

In this case, the non-zero eigenstresses can be written as:

$$\sigma^T_{12} = \sigma^T_{12} = \mu, \quad \sigma^T_{11} = \sigma^T_{22} = 0 \tag{A.15}$$

Then we can obtain the Airy stress function by the Eshelby theorem in the form

$$\psi^{12\infty} = \sigma^T_{12}\frac{\partial \phi^1}{\partial x'_2} + \sigma^T_{21}\frac{\partial \phi^2}{\partial x'_1} \tag{A.16}$$

Therefore, we have

$$\psi^{12\infty} = \frac{2\mu}{\pi(\kappa+1)}\frac{\sin 2\theta}{2} \tag{A.17}$$

where $\sin 2\theta = 2\xi\eta/r^2$. It is found that the forms of the Airy stress functions for edge and glide dislocation dipoles are exactly the same as those obtained by Dundurs (1968) and Korsunsky (1994) by using a differentiation method.

A.4 Green's functions for dislocation dipoles in infinite media

Based on the Airy stress functions obtained above for edge and gilding dislocation dipoles, we can obtain the Green's functions through the definition of the Airy stress functions. Let us denote the stresses by

$$\sigma_{ij\infty} = \frac{2\mu}{\pi(\kappa+1)}L^{kl}_{ij\infty}\Delta u_{kl} \tag{A.18}$$

where Δu_{kl} denotes the strength of dislocation dipoles. The detailed expressions of $L^{kl}_{ij\infty}$ can be found in Hills et al. (1996).

Appendix B: Green's functions for a dipole in bimaterials

Based on Aderogba (1977), we can derive the Airy stress functions for the bimaterial elasticity problems from their counterparts for full-plane problems. If there is no net forces on the internal boundaries, the elastic solutions depend on only two dimensionless Dundurs parameters α and β, defined as

$$\alpha = \frac{\mu_2(\kappa_1+1) - \mu_1(\kappa_2+1)}{\mu_2(\kappa_1+1) + \mu_1(\kappa_2+1)} \tag{B.1}$$

$$\beta = \frac{\mu_2(\kappa_1-1) - \mu_1(\kappa_2-1)}{\mu_2(\kappa_1+1) + \mu_1(\kappa_2+1)} \tag{B.2}$$

where μ_1, μ_2 are shear moduli and $\kappa_1 = 3 - 4\nu_1$, $\kappa_2 = 3 - 4\nu_2$ for the upper and lower half plane, respectively. Note that the choice of the constants is not unique. Following Aderogba (1977) for simplicity, we employed the elastic constants A and B are given by

$$A = \frac{\beta - \alpha}{1+\beta} \quad B = -\frac{\alpha+\beta}{1-\beta} \tag{B.3}$$

Assume that the dislocation dipoles are situated in material 1 and the corresponding Airy stress function in infinite elastic medium is denoted as

$\Phi_0(x_1, x_2, x_1', x_2')$. To meet the stress and displacement continuities across the interface, the new Airy stress function can be written as: for material 1

$$\Phi_1 = \Phi_0 + \Psi_1 \tag{B.4}$$

and for material 2,

$$\Phi_2 = \Phi_0 + \Psi_2 \tag{B.5}$$

where Ψ_1 and Ψ_2 are biharmonic functions. Substituting the Airy stress functions to the continuity conditions on the interface $x_2 = 0$

$$u_1^1 = u_1^2 \quad u_1^1 = u_1^2 \tag{B.6}$$
$$\sigma_{11}^1 = \sigma_{11}^2 \quad \sigma_{12}^1 = \sigma_{12}^2 \tag{B.7}$$

Observe that the solution to the biharmonic equation can be expressed as $\Phi_0(x_1, x_2, x_1', x_2') = \Phi_0(s, t)$ if $s = x_1 - x_1'$ and $t = x_2 - x_2'$. Therefore, $\Phi_0(x_1, x_2, -x_1', x_2') = \Phi_0(s, \bar{t})$ if $\bar{t} = x_2 + x_2'$. Following the observations by Aderogba (1977), the general solutions with each layer can be written in the form of an operator

$$\Psi_i = \hbar_i \Phi_0 \tag{B.8}$$
$$\hbar_i = A_i + B_i x_1 \frac{\partial}{\partial x_1} + C_i x_1^2 \nabla^2 + D_i x_1 \int \nabla^2 \, \mathrm{d}x_2 + E_i \int\int \nabla^2 \mathrm{d}x_2 \mathrm{d}x_2 \tag{B.9}$$

where the subscript i is used for reference to regions 1 and 2, and the associated coefficients are undetermined constants.

Substitute Ψ_1 and Ψ_2 into the continuity conditions and consider that the normal stresses caused by Φ_0 are the same on both sides of the interface, while the shear stresses have a sign convection. Manipulations of all terms in left-hand and right-hand sides of the continuity conditions, we can determine the unknown coefficients in Eq. (B.9). Finally, the operators of material 1 and 2 for edge dislocation dipoles are given by, respectively,

$$L_1 = -A\left[1 - 2x_2 \frac{\partial}{\partial x_1} + x_2^2 \nabla^2\right] - 0.25(A - B) \int\int \nabla^2 \, \mathrm{d}x_2 \mathrm{d}x_2 \tag{B.10}$$

$$L_2 = -A - 0.25(A - B) \times \left[\int\int \nabla^2 \, \mathrm{d}x_2 \mathrm{d}x_2 - 2x_2 \int \nabla^2 \, \mathrm{d}x_2\right] \tag{B.11}$$

It should be mentioned that the operators for glide dislocation dipoles are $-L_1$ and L_2.

B.1 Edge dislocation dipoles

The Airy stress function for an edge dislocation dipole in an infinite medium is $\psi^{11\infty}$. Therefore, the reflection part of the Airy stress function for an edge dislocation dipole in material 1 along the x_1 direction is

$$\psi^{11R} = \frac{2\mu_1}{\pi(\kappa_1 + 1)} \times \left[\frac{A + B}{2} \log \bar{r} - \frac{A}{2} \cos 2\bar{\theta} \left(1 + 4\frac{x_2 x_2'}{\bar{r}^2}\right)\right] \tag{B.12}$$

and the transmission part is

$$\psi^{11T} = \frac{2\mu_1}{\pi(\kappa_1 + 1)} \left[\left(-1 + \frac{A + B}{2}\right) \times \log r + \frac{1 - A}{2} \cos 2\theta - (A - B)\frac{\eta x_2'}{r^2}\right] \tag{B.13}$$

where $\bar{\eta} = x_2 + x_2', \bar{r} = \sqrt{\xi^2 + \bar{\eta}^2}, \bar{\theta} = \arctan[\bar{\eta}/\xi]$.

In the same way, the reflection part of the Airy stress function for an edge dislocation dipole in material 1 along the x_2 direction is

$$\psi^{22R} = \frac{2\mu_1}{\pi(\kappa_1 + 1)} \left[\frac{3A - B}{2} \log \bar{r} + \frac{A}{2} \cos 2\bar{\theta} \left(1 + 4\frac{x_2 x_2'}{\bar{r}^2}\right)\right] - 4A\frac{\bar{\eta} x_2'}{\bar{r}^2} \tag{B.14}$$

and the transmission part is

$$\psi^{22T} = \frac{2\mu_1}{\pi(\kappa_1 + 1)} \left[\left(-1 + \frac{A + B}{2}\right) \times \log r - \frac{1 - A}{2} \cos 2\theta - (A - B)\frac{\eta x_2'}{r^2}\right] \tag{B.15}$$

B.2 Glide dislocation dipoles

The Airy stress function for a glide dislocation dipole in an infinite medium is $\psi^{12\infty}$. Therefore, the reflection part of the Airy stress function for an glide dislocation dipole in material 1 is

$$\psi^{12R} = \frac{2\mu_1}{\pi(\kappa_1+1)}\left[-A\frac{\sin 2\bar{\theta}}{2} - 2A\frac{x_2'}{\bar{r}^2}(\xi\cos 2\bar{\theta} - x_1'\sin 2\bar{\theta}) - \frac{A-B}{2}\arctan\left(\frac{\xi}{\bar{\eta}}\right)\right] \quad \text{(B.16)}$$

and the transmission part is

$$\psi^{12T} = \frac{2\mu_1}{\pi(\kappa_1+1)}\left[(1-A)\frac{\sin 2\theta}{2} - (A-B)\frac{\eta x_2'}{r^2} - \frac{A-B}{2}\arctan\left(\frac{\xi}{\bar{\eta}}\right)\right] \quad \text{(B.17)}$$

Appendix C: Image method for three-layered media

C.1 A coordinate translation and transformation rules

Suppose that the interface between material 1 and 2 is perfectly bonded along $x_2' = H$. With a coordinate transition $x_2^* = x_2' - H$, the interface is reformated based on the new coordinate system with $x_2^* = 0$. If the singularity is situated in material 1, the material constants are defined as

$$A_{12} = \frac{\beta-\alpha}{1+\beta} \quad B_{12} = -\frac{\alpha+\beta}{1-\beta} \quad \text{(C.1)}$$

Therefore, the operators L_{112} and L_{212} are given by

$$L_{112} = -A_{12}\left[1 - 2\rho\frac{\partial}{\partial\hat{\eta}} + \rho^2\nabla^2\right] - 0.25(A_{12}-B_{12})\int\int\nabla^2\,\mathrm{d}\hat{\eta}\mathrm{d}\hat{\eta} \quad \text{(C.2)}$$

based on the substitutions

$$\hat{\eta} = x_2 + x_2' - 2H \quad \rho = x_2 - H \quad \text{(C.3)}$$

and

$$L_{212} = 1 - A_{12} - 0.25(A_{12}-B_{12}) \times\left[\int\int\nabla^2\,\mathrm{d}\eta\mathrm{d}\eta - 2\rho\int\nabla^2\,\mathrm{d}\eta\right] \quad \text{(C.4)}$$

C.1.1 Edge dislocation dipoles in 1-direction

The reflection part of the Airy stress function for an edge dislocation dipole in material 1 along the x_1 direction is

$$\psi_{12}^{11R} = \frac{2\mu_1}{\pi(\kappa_1+1)}\left[\frac{A_{12}+B_{12}}{2}\log\hat{r} - \frac{A_{12}}{2}\cos 2\hat{\theta}\left(1+4\frac{\rho(\hat{\eta}-\rho)}{\hat{r}^2}\right)\right] \quad \text{(C.5)}$$

and the transmission part is

$$\psi_{12}^{11T} = \frac{2\mu_1}{\pi(\kappa_1+1)}\left[\left(-1+\frac{A_{12}+B_{12}}{2}\right)\log r + \frac{1-A_{12}}{2}\cos 2\theta + (A_{12}-B_{12})\frac{\xi(\xi-\rho)}{r^2}\right] \quad \text{(C.6)}$$

where $\hat{r} = \sqrt{\xi^2+\hat{\eta}^2}, \hat{\theta} = \arctan[\hat{\eta}/\xi]$. It should be noted that x_2' should be replaced by $2H - x_2'$ for the position of the image point.

C.1.2 Edge dislocation dipoles in 2-direction

The reflection part of the Airy stress function for an edge dislocation dipole in material 1 along the x_2 direction is

$$\psi_{12}^{22R} = \frac{2\mu_1}{\pi(\kappa_1+1)}\left[\frac{3A_{12}-B_{12}}{2}\log\hat{r} + \frac{A_{12}}{2}\cos 2\hat{\theta}\left(1+4\frac{\rho(\hat{\eta}-\rho)}{\hat{r}^2}\right)\right] - 4A_{12}\frac{\hat{\eta}(\hat{\eta}-\rho)}{\hat{r}^2}\Bigg) \quad \text{(C.7)}$$

and the transmission part is

$$\psi_{12}^{22T} = \frac{2\mu_1}{\pi(\kappa_1+1)}\left[\left(-1+\frac{A_{12}+B_{12}}{2}\right)\log r - \frac{1-A_{12}}{2}\cos 2\theta - (A_{12}-B_{12})\frac{\eta(\hat{\eta}-\rho)}{r^2}\right] \quad \text{(C.8)}$$

C.1.3 Glide dislocation dipoles

The reflection part of the Airy stress function for an glide dislocation dipole in material 1 is

$$\psi_{12}^{12R} = \frac{2\mu_1}{\pi(\kappa_1+1)}\left\{-A_{12}\frac{\sin 2\hat{\theta}}{2} - 2A_{12}\frac{\hat{\eta}-\rho}{\hat{r}^2} \times[\xi\cos 2\hat{\theta} - (\hat{\eta}-\rho)\sin 2\hat{\theta}] - \frac{A_{12}-B_{12}}{2}\arctan\left(\frac{\hat{\eta}}{\xi}\right)\right\} \quad \text{(C.9)}$$

and the transmission part is

$$\psi_{12}^{12T} = \frac{2\mu_1}{\pi(\kappa_1+1)}\left[(1-A_{12})\frac{\sin 2\theta}{2} - (A_{12}-B_{12}) \times \frac{\eta(\hat{\eta}-\rho)}{r^2} - \frac{A_{12}-B_{12}}{2}\arctan\left(\frac{\hat{\eta}}{\xi}\right)\right] \tag{C.10}$$

Upon obtaining the Airy stress functions, the stress components associated with the specified singularity can be determined by Eq. (5).

C.2 Image method

Consider a singularity embedded in the three-layered materials, which have two parallel interfaces. It is known that there are infinite images for this problem. One possible way to solve this problem has been proposed by Aderogba (2003), which resembles the Schwarz–Neumann's alternating in complex variable theory with analytical continuity across interfaces (see Choi and Earmme 2002). Since it is difficult to meet the continuity conditions along two interfaces simultaneously, the continuity can be applied to each interface alternatively disregarding the existence of the another interface. This is the basis of the image method to deal with an infinite series of images.

The introduction about the implementation of the image method has been described in Section 2. Without loss of generality, let us consider the case when the singularity is located within the interlayer. With regard to $x_2 = 0$, the corresponding Airy stresses functions for the first order image have been given in the last subsection. Then, let us consider the images with respect to $x_2 = H$. Introducing the coordinate translation $x_2^{**} = x_2' + H$, we can obtain the Airy stress functions for the singularity source based on the above formulation. But we need to consider the image induced by the first order image. It must be noted that the strength of the second-order image is not the full-plane solution, but the reflection part of Airy stress function with regards to $x_2 = 0$ after replacing $\hat{\eta}$ by η. Repeat this procedure for the image with respect to $x_2 = 0$ based on Eqs. (C.2) and (C.4) and add its contribution to the full-plane Airy stress function. It should be mentioned that the undisturbed Airy stress function for the third order image is also the reflection part of Airy stress function for the second-order image after replacing $\hat{\eta}$ by η.

Appendix D: General expressions for equations of equilibrium

Following Hills et al. (1996), we rewrite the equation of equilibrium in an alternative way based on the influence functions for dislocation dipoles

$$\frac{\pi(\kappa_2+1)}{2\mu_2}\sigma_{ij}(\mathbf{x}^m) = \sum_{m=1}^{M}\int_0^{l_m}\{L_{ij}^{11}(\mathbf{x}^m,\mathbf{x}^n,\alpha,\beta)b_{11}(\mathbf{x}^n) + L_{ij}^{22}(\mathbf{x}^m,\mathbf{x}^n,\alpha,\beta)b_{22}(\mathbf{x}^n) + L_{ij}^{12}(\mathbf{x}^m,\mathbf{x}^n,\alpha,\beta)[b_{12}(\mathbf{x}^n) + b_{21}(\mathbf{x}^n)]\}\,\mathrm{d}s(\mathbf{x}^n) \tag{D.1}$$

in which b_{ij} is the strength of the dipole, which is the negative crack opening/sliding displacement in the ith direction measured in the direction normal to j.

For convenience in implementing the numerical method, the stress components should be expressed in the local coordinate system at node m and the strength of the dipole expressed in the local coordinate system at node n. To this end, the stress components in the global set are first expressed in terms of the local dipole strength in local coordinates of node n. Then the stress components are transformed into the local coordinate system at node m. According to the transformation of the tensor of rank 2, we find that

$$\begin{Bmatrix} b_{11} \\ b_{22} \\ b_{12}+b_{21} \end{Bmatrix} = \mathbf{A}\begin{Bmatrix} \hat{b}_{11} \\ \hat{b}_{22} \\ \hat{b}_{12}+\hat{b}_{21} \end{Bmatrix} \tag{D.2}$$

in which the 3×3 matrix $\mathbf{A}$ is

$$\mathbf{A} = \begin{bmatrix} \cos^2\theta_n & \sin^2\theta_n & -\sin\theta_n\cos\theta_n \\ \sin^2\theta_n & \cos^2\theta_n & -\sin\theta_n\cos\theta_n \\ \sin^2\theta_n & -\sin^2\theta_n & \cos^2\theta_n \end{bmatrix} \tag{D.3}$$

We now insert it in (D.1), the new influence functions in the local set are obtained as follows

$$\begin{bmatrix} \hat{L}_{11}^{11} & \hat{L}_{11}^{22} & \hat{L}_{11}^{12} \\ \hat{L}_{22}^{11} & \hat{L}_{22}^{22} & \hat{L}_{22}^{12} \\ \hat{L}_{12}^{11} & \hat{L}_{12}^{22} & \hat{L}_{12}^{12} \end{bmatrix} = \begin{bmatrix} L_{11}^{11} & L_{11}^{22} & L_{11}^{12} \\ L_{22}^{11} & L_{22}^{22} & L_{22}^{12} \\ L_{12}^{11} & L_{12}^{22} & L_{12}^{12} \end{bmatrix}\mathbf{A} \tag{D.4}$$

The non-zero components of dipole strength in the local set are $\hat{b}_{12}$ and $\hat{b}_{22}$. Hence, we have

$$\frac{\pi(\kappa+1)}{2\mu}\sigma_{ij}(\mathbf{x}^m) = \sum_{m=1}^{M}\int_0^{l_m}\{\hat{L}_{ij}^{22}(\mathbf{x}^m,\mathbf{x}^n,\alpha,\beta)\hat{b}_{22}(\mathbf{x}^n) + \hat{L}_{ij}^{12}(\mathbf{x}^m,\mathbf{x}^n,\alpha,\beta)\hat{b}_{12}(\mathbf{x}^n)\}\,\mathrm{d}s(\mathbf{x}^n) \tag{D.5}$$

The next step is to evaluate the normal and shear stresses in the local coordinate system of node m. This can be achieved by the stress transformation

$$\begin{Bmatrix}\tilde{\sigma}_{11}\\ \tilde{\sigma}_{22}\\ \tilde{\sigma}_{12}\end{Bmatrix} = \mathbf{A}^{\mathrm{T}}\begin{Bmatrix}\sigma_{11}\\ \sigma_{22}\\ \sigma_{12}\end{Bmatrix} \tag{D.6}$$

in which $\mathbf{A}^{\mathrm{T}}$ is the transpose of $\mathbf{A}$.

Finally, the equation of equilibrium of traction along the fracture is written as

$$\frac{\pi(\kappa+1)}{2\mu}\tilde{\sigma}_{ij}(\mathbf{x}^m) = \sum_{m=1}^{M}\int_0^{l_m}\{\tilde{L}_{ij}^{22}(\mathbf{x}^m,\mathbf{x}^n,\alpha,\beta)\tilde{b}_{22}(\mathbf{x}^n) + \tilde{L}_{ij}^{12}(\mathbf{x}^m,\mathbf{x}^n,\alpha,\beta)\hat{b}_{12}(\mathbf{x}^n)\}\,\mathrm{d}s(\mathbf{x}^n) \tag{D.7}$$

in which the two-point influence functions are defined as

$$\begin{bmatrix}\tilde{L}_{11}^{11} & \tilde{L}_{11}^{22} & \tilde{L}_{11}^{12}\\ \tilde{L}_{22}^{11} & \tilde{L}_{22}^{22} & \tilde{L}_{22}^{12}\\ \tilde{L}_{12}^{11} & \tilde{L}_{12}^{22} & \tilde{L}_{12}^{12}\end{bmatrix} = \mathbf{A}^{\mathrm{T}}\begin{bmatrix}L_{11}^{11} & L_{11}^{22} & L_{11}^{12}\\ L_{22}^{11} & L_{22}^{22} & L_{22}^{12}\\ L_{12}^{11} & L_{12}^{22} & L_{12}^{12}\end{bmatrix}\mathbf{A} \tag{D.8}$$

References

Aderogba K (1977) On eigenstresses in dissimilar media. Phil Mag 35(2):281–292

Aderogba K (2003) An image treatment of elastostatic transmission from an interface layer. J Mech Phys Solids 51:267–279

Akisanya AR, Fleck NA (1992) Analysis of a wavy crack in sandwich specimens. Int J Fracture 55:29–45

Chai H (1987) A note on crack trajectory in an elastic strip bounded by rigid substrates. Int J Fracture 32:211–213

Chan HM (1997) Layered ceramics: processing and mechanical behavior. Annu Rev Mater Sci 27:249–282

Choi ST, Earmme YY (2002) Elastic study on singularities interacting with interfaces using alternating technique: part II isotropic trimaterial. Int J Solids Structures 39:1199–1211

Delaney PT, Pollard DD, Ziony JI, McKee EH (1986). Field relations between dikes and joints: emplacement processes and paleostress analysis. J Geophys Res 91:4920–4938

Dundurs J (1968) Analogy between concentrated forces and edge dislocations. J Appl Phys 39:4152–4156

Erdogan F, Sih GC (1963) On the crack extension in plates under plane loading and transverse shear. J Basic Eng 519–527

Fett T, Munz D (1997) Stress intensity factors and weight functions. Computational Mechanics Publications

Fleck NA, Hutchinson JW, Suo Z (1991) Crack path selection in a brittle adhesive layer. Int J Solids Structures 27:1683–1703

Folsom CA, Zok FW, Lange FF (1994). Flexural properties of brittle multilayer materials: I, modeling. J Am Ceram Soc 77:689–696

He MY, Bartlett AA, Evans AG, Hutchinson JW (1991) Kinking of a crack out of an interface: role of in-plane stress. J Am Ceram Soc 74:767–771

Hills D, Kelly P, Dai D, Korsunsky A (1996) Solution of crack problems. The distributed dislocation technique, Vol. 44 of solid mechanics and its applications. Kluwer Academic Publications Dordrecht

Hilton PD, Sih GC (1971) A laminate composite with a crack normal to the interfaces. Int J Solids Structures 7:913–930

Hutchinson JW, Mear ME, Rice JR (1987) Crack paralleling an interface between dissimilar materials. ASME J Appl Mech 54:828–832

Hutchinson JW, Suo Z (1992) Mixed mode cracking in layered materials. Adv Appl Mech 29:63–191

Korsunsky AM (1994) The solution of axisymmetric crack problems in inhomogeneous media. Ph. D. thesis, Oxford University

Lu TJ (1996) Crack branching in all-oxide ceramic composites. J Am Ceram Soc 79:266–274

Mura T (1987) Micromechanics of defects in solids. Martinus Nijhoff Publishers, Dordrecht

Peirce A, Siebrits E (2001) Uniform asymptotic approximations for accurate modeling of cracks in layered elastic media. Int J Fracture 110:205–239

Pollard DD, Aydin A (1988) Progress in understanding jointing over the past century. Geol Soc Am Bull 100:1181–1204

Price NJ, Cosgrove JW (1990) Analysis of geological structures. Cambridge University Press, Cambridge, UK

Suiker ASJ, Fleck NA (2004) Crack tunneling and plane-strain delamination in layered solids. Int J Fracture 125:1–32

Suo Z, Hutchinson JW (1989) On sandwich test specimen for measuring interface crack toughness. Mater Sci Eng A107:135–143